Chapter 10
Resonators I: Basic Theory

10.1 INTRODUCTION

In previous chapters, we investigated the configuration in which a piezoelectric transducer was rigidly attached to a substrate with a thickness much greater than that of the piezolayer. The substrate could be, but was not required to be, piezoelectrically active. The bandwidth and energy conversion of electric to acoustic energy depended on the acoustic and electrical properties of all layers in the acoustic path. The goal in this structure is to increase the bandwidth (and thus reduce the Q) by choosing transducers with high coupling constant that were well matched acoustically to the substrate.

In this chapter, we investigate a different type of device in which the acoustic wave is confined to the transducer layer. The goal in this case is to produce a device with very narrow bandwidth and high Q. Called a *resonator,* this structure utilizes the same high-quality piezoelectric single crystals considered in the previous chapters. Resonator performance is optimized by choosing crystals with low attenuation. The coupling constant also plays an important role by allowing an increase in the range of resonator frequencies.

Traditionally, resonators have been excited with the external electric field parallel to the resonator plate normal (thickness excitation, TE). Recently, however, excitation in which the exciting field is perpendicular to the plate normal (lateral field excitation) has been receiving more attention. We investigate both of these configurations from fundamental acoustic principles, and we discuss the advantages of each. We develop equivalent circuits that represent the crystal resonator near the resonance frequencies, and we derive the values of the circuit elements in terms of fundamental acoustic and electrical parameters (attenuation, phase velocity, etc.). Finally, we discuss the properties of the important resonator

material crystal quartz, and briefly investigate the stability of resonators with temperature. These discussions do not exhaustively investigate resonator techniques, but illustrate an important application of crystal bulk acoustics.

10.2 THICKNESS EXCITATION OF ACOUSTIC TRANSDUCERS

Consider the structure shown in Figure 10.1. We showed in Chapter 4 that for an acoustic wave propagating in a piezoelectric medium there is a longitudinal electric field but that the longitudinal displacement vector was zero. If the piezoelectric crystal consists of a thin electrode medium as in Figure 10.1, this result is equally valid. Indeed, it is easy to show that the displacement is precisely zero (i.e., there are no lateral components and no longitudinal component). To do this, we write the electric field from (9.35),

$$E_j = \frac{-l_j l_i e_{iL} S_L}{l_i l_j \epsilon_{ij}^{\mathbf{S}}}$$

Thus, we write

$$\mathbf{D} = \boldsymbol{\epsilon}:\mathbf{E} + \mathbf{e}:\mathbf{S}$$

or

$$D_i = \epsilon_{ij}^{\mathbf{S}} E_j + e_{iL} S_L \tag{10.1}$$

Substituting E_j from (9.35) into (10.1), we obtain $\mathbf{D} = 0$. Because the displacement is zero, acoustic wave propagation in this configuration requires that we use $\mathbf{c}^{\mathbf{D}}$ in place of $\mathbf{c}^{\mathbf{E}}$, where

$$\mathbf{c}^{\mathbf{D}} = \frac{e^2}{\epsilon^{\mathbf{S}}} + \mathbf{c}^{\mathbf{E}}$$

Thus, the coupling constant valid for this structure is found to be

$$k_i^2 = \frac{e^2}{\epsilon^{\mathbf{S}} c^{\mathbf{D}}} = \frac{K^2}{K^2 + 1}$$

where

$$K^2 = \frac{e^2}{c^{\mathbf{E}}\epsilon^{\mathbf{S}}}$$

Example 10.1 Show that the displacement is identically zero for the $\langle z \rangle$-cut of barium sodium niobate ($Ba_2NaNb_5O_{15}$). In Example 4.3, we found that the electric field was given by

$$\mathbf{E} = -\frac{e_{33}}{\epsilon_{33}}\hat{\mathbf{k}}$$

Using (10.1), we write

$$\boldsymbol{\epsilon}:\mathbf{E} = -e_{33}\hat{\mathbf{k}}, \quad \mathbf{e}:\mathbf{S} = \begin{bmatrix} 0 & 0 & 0 & 0 & e_{15} & 0 \\ 0 & 0 & 0 & e_{24} & 0 & 0 \\ e_{31} & e_{32} & e_{33} & 0 & 0 & 0 \end{bmatrix} \begin{bmatrix} 0 \\ 0 \\ 1 \\ 0 \\ 0 \\ 0 \end{bmatrix} = e_{33}\hat{\mathbf{k}}$$

Because the displacement vector is the sum of these two terms, it is indeed zero.

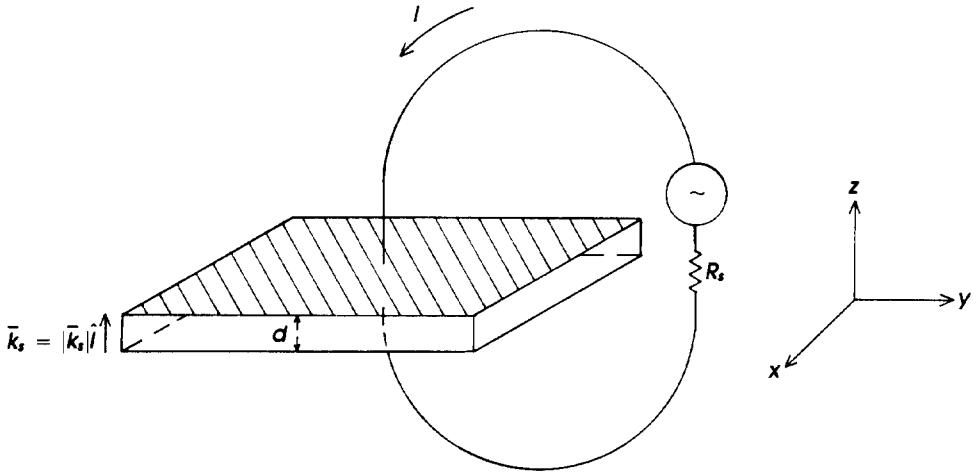

Figure 10.1 Thickness excitation of piezoelectric resonator. In TE, the electric field is in the direction of acoustic wave propagation.

The voltage-current relation in this configuration is derived by assuming that the displacement current depend only on the external source, because there was no acoustically generated **D**. The total *electric* field is the sum of the external and acoustically generated fields, as given by (5.25),

$$E = \frac{D_z}{\epsilon^S} - \frac{e}{e^S} S$$

where the first term is the contribution of the "dead" capacitor, and the second term represents the interaction of the external field with the acoustic wave. We obtain the voltage across the piezolayer by integrating the electric field of (5.25).

The Mason model equations for the transducer are then

$$0 = Z_T\left(\frac{v_1}{j\tan(kd)} - \frac{v_2}{j\sin(kd)}\right) + \frac{h}{j\omega} I \tag{10.2}$$

$$-Z_S v_2 = Z_T\left(\frac{v_1}{j\sin(kd)} - \frac{v_2}{j\tan(kd)}\right) + \frac{h}{j\omega} I \tag{10.3}$$

$$V = \frac{h}{j\omega}(v_1 - v_2) + \frac{I}{j\omega C_0} \tag{10.4}$$

In (10.2) to (10.4), we note that the current I is an independent variable, reflecting the fact that the electric field is composed of external and acoustically generated components, whereas **D** depends only on the source. The form of (10.4) results in the appearance of a negative capacitance in the equivalent circuit (Figure 5.5(b)).

In a resonator, the piezoelectric layer is bounded by an acoustic short circuit (vacuum or air) on *both* sides; i.e., $Z_S \rightarrow 0$. Equation (10.3) becomes

$$0 = Z\left(\frac{v_1}{j\sin(kd)} - \frac{v_2}{j\tan(kd)}\right) + \frac{h}{j\omega} I \tag{10.5}$$

We drop the subscript because the transducer is the only impedance. Equations (10.2) and (10.3) have the form:

$$\begin{aligned} ax + by &= -c \\ bx + ay &= -c \end{aligned} \tag{10.6}$$

where

$$a = \frac{Z}{j\tan(kd)}, \quad b = \frac{Z}{j\sin(kd)}, \quad c = \frac{h}{j\omega}$$

$$x = \frac{v_1}{I}, \quad y = \frac{v_2}{I}$$

The solution of the coupled system (10.6) is

$$\begin{aligned} x &= \frac{v_1}{I} = \frac{-c}{a+b} = y \\ &= \frac{-h/j\omega}{Z/(j\tan(kd)) + Z/(j\sin(kd))} \end{aligned} \tag{10.7}$$

As in the infinite delay line structure (Figure 5.7), there are four unknowns: the two particle velocities v_1 and v_2 at the boundaries, and the electrical variables V and I. We solve the system of three equations for the ratio $V/I = Z_{in}$. From (10.4), the input impedance is

$$\begin{aligned} Z_{in} &= \frac{V}{I} = \frac{h}{j\omega}(x - y) + \frac{1}{j\omega C_0} \\ &= \frac{-2h^2}{j\omega^2 Z}\left(\frac{1}{1/\tan(kd) + 1/\sin(kd)}\right) + \frac{1}{j\omega C_0} \end{aligned} \tag{10.8}$$

Using the trigonometric identity:

$$\cot\left(\frac{\theta}{2}\right) = \frac{1}{\sin\theta} + \frac{1}{\tan\theta} \tag{10.9}$$

in (10.8), we get

$$Z_{in} = \frac{1}{j\omega C_0}\left(1 - \frac{2C_0h^2}{\omega Z}\tan\left(\frac{kd}{2}\right)\right) \tag{10.10}$$

Finally, the coefficient of the tangent term can be written in the form,

$$\begin{aligned} \frac{C_0h^2}{\omega Z} &= \left(\frac{\epsilon^s A}{d}\frac{e^2}{\epsilon^2}v_a\right)\Big/\omega c^D A \\ &= \frac{k_t^2 v_a}{\omega d} = \frac{k_t^2}{kd} \end{aligned} \tag{10.11}$$

Substituting (10.11) into (10.10) gives

$$Z_{\text{in}} = \frac{1}{j\omega C_0}\left(1 - k_t^2 \frac{\tan(kd/2)}{kd/2}\right) \tag{10.12}$$

In this configuration, the input impedance is reactive for all frequencies. The radiation resistance is zero, and there is no conversion from electrical to acoustic energy, even with a large coupling constant. The piezoelectric medium, however, is not "dead." There is an acoustic contribution that is proportional to k_t^2. The existence of the acoustic term causes the input impedance to move into the inductive region of the Smith chart. The larger k_t^2 is, the wider is the frequency band for which Z_{in} is inductive. The resonator is most useful in the inductive region. We will return to (10.12) after we investigate a variation in the excitation called LFE.

10.3 LATERAL FIELD EXCITATION

Consider the configuration of Figure 10.2, where the applied electric field is uniform in the y direction and the acoustic propagation is in the z direction (perpendicular to the electric field). The electrical source does not directly cause a displacement vector (and thus there is no displacement current) in the direction of propagation. An electric field can excite an acoustic wave normal to its direction because the piezoelectric matrix couples electrical and mechanical fields of varying orientations. Consider, for example, barium sodium niobate oriented for acoustic propagation in the z direction. In TE, we found that a z-directed electric field resulted in a longitudinal acoustic wave through the piezoelectric coefficient e_{33}. In the present configuration, we require that the external field be *normal* to the z-axis, as shown in Figure 10.2.

For a z-directed wave, the three possible stress components are T_3 (longitudinal wave), T_4 (shear wave with y-polarization), and T_5 (shear wave with x-polarization). For a z-propagating acoustic wave, the relation between the stress and electric field is of the form:

$$\begin{bmatrix} 0 & 0 & e_{31} \\ 0 & 0 & e_{32} \\ 0 & 0 & e_{33} \\ 0 & e_{24} & 0 \\ e_{15} & 0 & 0 \\ 0 & 0 & 0 \end{bmatrix} \begin{bmatrix} E_x \\ E_y \\ E_z \end{bmatrix} = \begin{bmatrix} 0 \\ 0 \\ T_3 \\ T_4 \\ T_5 \\ 0 \end{bmatrix} \tag{10.13}$$

Because the field is necessarily perpendicular to the propagation direction, we require $E_z = 0$. From (10.13), it is clear that only shear modes are excited; T_4 couples with E_y (through e_{24}), and T_5 couples with E_x (through e_{15}). It would have been possible to excite a longitudinal mode had the components e_{13} or e_{23} been nonzero. For the $\langle z \rangle$-cut in this crystal, TE resulted in a longitudinal wave, whereas LFE resulted in a shear wave. This behavior is typical. If TE results in a shear wave, LFE will probably result in a longitudinal wave, and *vice versa*.

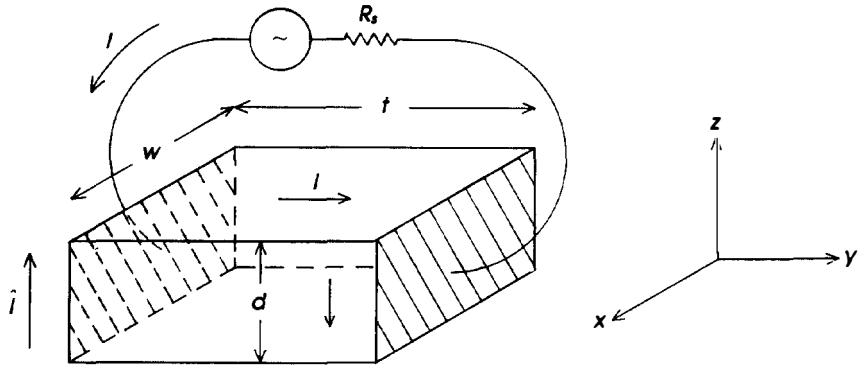

Figure 10.2 Lateral field excitation of piezoelectric resonator. In LFE, the electric field is in the plane perpendicular to acoustic propagation.

For a given stress to be excited by orthogonal field components (i.e., for TE and LFE modes to exist for a given acoustic mode) requires that the piezoelectric matrix contain nonzero elements for a given row in adjacent columns (e.g., e_{33} must be associated with a nonzero e_{13} or e_{23}). For cubic, tetragonal (classes $4mm$, $\bar{4}2m$, and $4mm$), orthorhombic, and trigonal 32 (of which crystal quartz is a member), this condition is not fulfilled. Of the important piezoelectric crystal classes, only in trigonal $3m$ (lithium niobate, $LiNbO_3$) are there principal axis directions for which both TE and LFE modes are excited. For off-axis propagation, an electric field may excite both types of modes, however (we will give an example in quartz later), because in a rotated system the piezoelectric matrix can have all components nonzero. Equally important is the fact that in LFE the electromechanical coupling can be just as robust as in TE, because in both TE and LFE the coupling between electrical and mechanical variables

occurs through the same piezoelectric matrix. Indeed, we will see examples in Chapter 11 of extremely high coupling constants in the LFE mode.

We found that if the piezoelectric transducer was attached to a substrate and excited in the TE mode, then the electrical source interacts (converts electrical into acoustic energy) with the acoustic wave through the acoustically generated longitudinal electric field and there was no acoustically generated displacement current. In the resonator structure, there is no energy conversion (the return loss is zero for all frequencies), but here is an electrical-acoustic interaction that causes the impedance characteristic to look inductive. Lateral field excited structures exhibit similar behavior with one important difference. Using the example of z-cut barium sodium niobate, we write the potential from (4.45):

$$\phi = \frac{l_i e_{iL} S_L}{\epsilon_{33}}$$

where for the $\langle z \rangle$-cut S_L is either S_4 or S_5 and l_i (direction of propagation) is (0, 0, 1). From (10.13), the product $e_{iL}S_L$ is given by

$$\begin{bmatrix} 0 & 0 & 0 & 0 & e_{15} & 0 \\ 0 & 0 & 0 & e_{24} & 0 & 0 \\ e_{31} & e_{32} & e_{33} & 0 & 0 & 0 \end{bmatrix} \begin{bmatrix} 0 \\ 0 \\ 0 \\ S_4 \\ S_5 \\ 0 \end{bmatrix} = \begin{bmatrix} e_{15}S_5 \\ e_{24}S_4 \\ 0 \end{bmatrix} \tag{10.14}$$

Carrying out the dot product ($l_i e_{iL} S_L$), we find immediately that $\phi = 0$! In lateral field excited modes, there is no internally generated electric field. Instead, there is an internally generated displacement vector normal to the direction of acoustic propagation. We can easily show this by writing (10.1):

$$D_i = \epsilon_{ij}E_j + e_{iL}S_L \tag{10.15}$$

$\epsilon_{ij}E_j$: from external electric field; $e_{iL}S_L$: generated by acoustic wave

The internally generated displacement vector is given by (10.14) and contains terms that are normal to the propagation direction and thus parallel to the exciting electric field. For a y-directed field, the displacement is proportional to $e_{24}S_4$, and for an x-directed field, it is proportional to $e_{15}S_5$ (compare with (10.13)). The interaction of the electrical source with the

acoustic wave takes place through the acoustically generated displacement vector rather than through the acoustically generated electric field, as in TE (which in this case does not exist). Because the (external) electric field is constant, the stiffness constant is $c^{\mathbf{E}}$ in the LFE structure, and the coupling constant is K^2 rather than k_t^2.

As in TE, for both wideband and resonator structures in LFE the existence of a normal displacement is independent of the boundary conditions on the piezoelectric crystal (if we assume that the thickness in the propagation direction is much less than the lateral dimensions). Like the TE case, it is the finite thickness of the transducer that results in the required resonance conditions. Furthermore, nothing in this analysis prevents LFE transducers in wideband applications from being rigidly attached to a substrate on one side of the piezoelectric body.

From a fabrication perspective, however, the ground plane (which is part of the TE structure) serves an important function. In sputtered piezoelectric film technology, the ground plane provides an ordered growth "bed" for the ZnO film, and in bonded transducer technology, it is the "glue" that holds the transducer to the substrate. In an LFE structure, the presence of a metallic layer between the transducer and the substrate would probably degrade device performance. It is not clear that an acoustic wave can be transferred directly from a transducer to a substrate without an intermediate metallic layer. If the acoustic wave in the substrate is piezoelectrically active, then the propagation is governed by the principles discussed in Chapter 4 and does not depend on the modes of excitation in the transducer. There will be a longitudinally directed electric field and no longitudinal displacement vector. The stiffness constant is $c^{\mathbf{D}}$. There is no interaction with an electrical source because there is no external field. There is, however, a coupling constant K^2. Table 10.1 summarizes the fields in TE and LFE in piezoelectric transducers.

For LFE, the electromechancial equations must be modified to reflect the fact that **E** rather than **D** is the independent variable. The mechanical—electrical equation now is

$$\mathbf{T} = \mathbf{c}:\mathbf{S} - \mathbf{e}:\mathbf{E} \rightarrow F = cAS - \frac{eVA}{t}$$

where the dimension t is defined in Figure 10.2 and V is the applied voltage. Equations (10.2) and (10.3) become

$$0 = Z\left(\frac{v_1}{j\tan(kd)} - \frac{v_2}{j\sin(kd)}\right) + \frac{AeV}{t} \tag{10.16}$$

$$0 = Z\left(\frac{v_1}{j\sin(kd)} - \frac{v_2}{j\tan(kd)}\right) + \frac{AeV}{t} \tag{10.17}$$

Table 10.1

Thickness Excitation	*Lateral Field Excitation*
Internally generated longitudinal **E** parallel to exciting field	Internally generated **D** parallel to exciting field
E propagates at the acoustic velocity	**D** propagates at the acoustic velocity
Interaction of the acoustic wave with source through **E**	Interaction of the acoustic wave with source through **D**
Stiffness components are measured at constant **D**	Stiffness components are measured at constant **E**
Coupling constant is k_t^2	Coupling constant is K^2

To write (10.4) with the voltage as independent variable, we first must solve for the current in terms of V (compared with the TE case where V was expressed in terms of I). Using (5.24), we write (assuming I is uniform across width)

$$I = j\omega W \int_0^d D \, dz \tag{10.18}$$

Substituting for D from (10.1), we get

$$I = j\omega W \int_0^d \left(\epsilon^s E_y + e\frac{\partial u}{\partial z}\right) dz \tag{10.19}$$

where the cross-sectional area $A = Wd$ (Figure 10.2). As in (10.13), the first term represents the contribution of the external (y-directed) field, and the second term is the acoustically generated component ($e_{24}S_4$ in (z) barium sodium niobate). If we assume that E_y is uniform across the crystal width, the integral immediately collapses to

$$I = \frac{j\omega VWd\epsilon^s}{t} + j\omega We\,(u_2 - u_1) \tag{10.20}$$

From Figure 10.2;

$$C_0 = \frac{Wd\epsilon^s}{t} \tag{10.21}$$

so (10.20) becomes

$$I = j\omega C_0 V + We(v_2 - v_1) \tag{10.22}$$

Our task is to solve the system of equations (10.16), (10.17), and (10.22). Because the voltage appears as the independent variable in this system, it is easier to find the input admittance. From (10.22),

$$Y_{\text{in}} = \frac{I}{V} = j\omega C_0 + We\left(\frac{v_2}{V} - \frac{v_1}{V}\right) \tag{10.23}$$

Dividing (10.16) and (10.17) by V and rearranging puts the equations in the form:

$$\begin{aligned} ax - by &= -c \\ bx - ay &= -c \end{aligned} \tag{10.24}$$

where (compare with (10.6))

$$a = \frac{Z}{j\tan(kd)}, \quad b = \frac{Z}{j\sin(kd)}, \quad c = \frac{Ae}{t}$$

and

$$x = \frac{v_1}{V} \quad \text{and} \quad y = \frac{v_2}{V}$$

The solution of (10.24) is (compare with (10.7))

$$x = \frac{-c}{a+b} = \frac{Ae}{t} \Big/ \left[\frac{Z}{j\tan(kd)} + \frac{Z}{j\sin(kd)}\right] = y \tag{10.25}$$

Substituting (10.24) into (10.23), we get

$$Y_{in} = \frac{I}{V} = j\omega C_0\left(1 - \frac{2We}{j\omega C_0}\left(\frac{Ae}{jZt}\right)\left[\frac{1}{\tan(kd)} + \frac{1}{\sin(kd)}\right]^{-1}\right)$$

$$= j\omega C_0\left(1 + \frac{2WAe^2}{\omega C_0 Zt}\tan\left(\frac{kd}{2}\right)\right) \tag{10.26}$$

where we used (10.9). Simplifying the coefficient of the tangent function, we have

$$\frac{2WAe^2}{\omega C_0 Zt} = 2WAe^2 \Big/ \omega\frac{Wd\epsilon^s}{t}\frac{Ac^E}{v_a}t = \frac{2e^2 v_a}{\epsilon^s c^E d} = \frac{K^2}{kd/2} \tag{10.27}$$

In (10.27), we used the coefficient c^E rather than c^D, reflecting the fact that the electric field is constant over z (this gives the coupling constant K^2 in (10.27). Substituting (10.27) into (10.26) gives

$$Y_{in} = j\omega C_0\left(1 + K^2\frac{\tan(kd/2)}{kd/2}\right) \tag{10.28}$$

Like the TE resonator configuration, LFE exhibits a purely reactive characteristic, and thus there is no conversion from electrical to acoustic energy. There is an inductive region, due to the presence of the acoustic term, with a strength proportional to K^2 (compared with k_t^2) and half-wave resonance conditions due to the $\tan(kd)$ term.

There is another important difference between LFE and TE. Recall that the equivalent circuit for the thickness-excited waves possessed a negative (nonphysically realizable) capacitor in the electrical port (see Figure 5.5). The presence of this element was required by the form of (5.28) and (5.30). In the LFE case, we write the corresponding equation with voltage as the independent variable:

$$F_1 = \frac{Z}{j\sin(kd)}(v_1 - v_2) + jZ\tan\left(\frac{kd}{2}\right)v_1 + \frac{Ae}{d}V \tag{10.29}$$

The equivalent circuit for this acoustoelectrical equation is shown in Figure 10.3. Note that from (10.29);

$$V_{cd} = \frac{Ae}{d}V \tag{10.30}$$

We determine the electrical-to-acoustic transformer turns ratio by inspecting (10.22):

$$\phi = We \tag{10.31}$$

Therefore, the voltage V_{ab} is

$$V_{ab} = \frac{V_{cd}}{\phi} = \frac{V_{cd}}{We} = \frac{AeV}{dWe} = V$$

because $Wd = A$. Because V is the voltage at the electrical port, the circuit does not possess a negative C_0. This conclusion does not imply that LFE is more "physical" than TE, but only that a physically unrealizable element is not required in the electrical model.

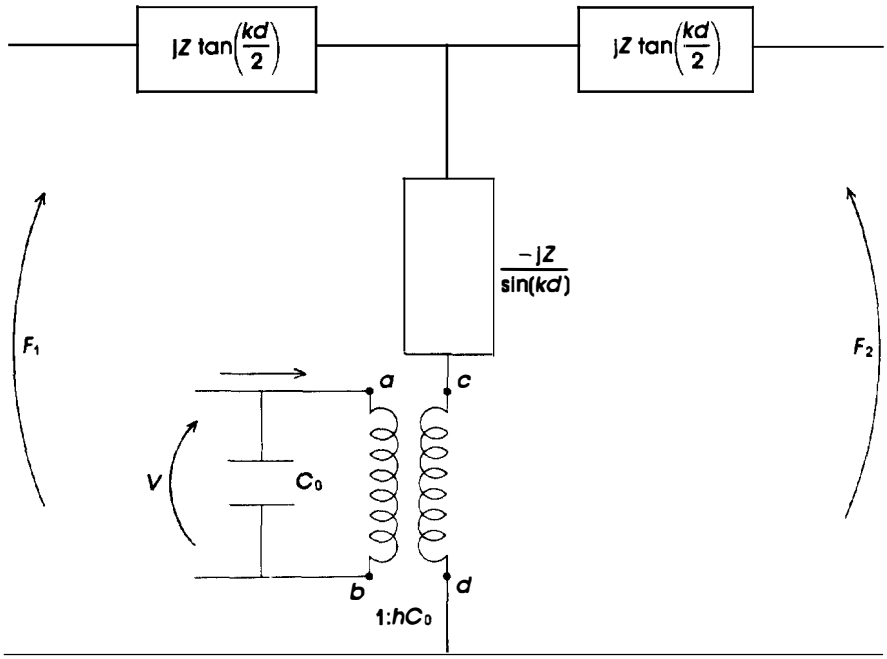

Figure 10.3 Equivalent circuit of piezoelectric layer in LFE mode. Compared with Figure 5.5, note the absence of the negative capacitor in the electrical port.

Although the configuration shown in Figure 10.2 permits a relatively simple computation of the clamped capacitance, it is not a practical structure. Because the acoustic thickness d is about half the acoustic wavelength,

d will generally be much smaller than the other dimensions. A more practical geometry is shown in Figure 10.4. Even at the relatively low frequency of 10 MHz, for example, d will typically be about .1 mm, whereas t' may be 1 to 5 mm. The capacitance C_0 is determined in part by the electrode width W and gap t', but in this configuration the exact determination of C_0 is usually quite difficult. In very high dielectric constant materials (especially ferroelectric materials), the electric field is nearly completely confined to the dielectric and C_0 is given by

$$C_0 = \frac{\epsilon_r \epsilon_0 W d}{t'} \tag{10.32}$$

The ratio d/t' is typically quite small and tends to remain constant, or even decrease, with frequency, in sharp contrast to the thickness-excited modes in which C_0 increases dramatically with frequency. This behavior will have important implications later.

Example 10.2. Calculate the clamped capacitance of a SiO_2 (AT)-cut resonator in TE and LFE at 10 MHz. For this important orientation, the phase velocity is 3.2×10^3 m/s. For TE modes,

$$C_0 = \frac{\epsilon_r \epsilon_0 A}{d} = \frac{4.5 \times 8.85 \times 10^{-12} \times 1 \times 10^{-6}}{1.6 \times 10^{-4}} = .25 \text{ pF}$$

assuming that the transducer dimensions are 1 mm by 1 mm. For the LFE mode, we choose $W = .5$ cm and $t' = 2$ mm. Using (10.32), we find $C_0 = .015$ pF.

We summarize the two important resonator relations:

$$Z_{\text{in}} = \frac{1}{j\omega C_0}\left(1 - k_t^2 \frac{\tan(\theta/2)}{\theta/2}\right)(\text{TE})$$

$$Y_{\text{in}} = j\omega C_0\left(1 + K^2 \frac{\tan(\theta/2)}{\theta/2}\right)(\text{LFE})$$

where

$$\theta = kd \quad \text{and} \quad k = \frac{\omega}{v_a} \tag{10.33}$$

In the wideband delay line configuration, the piezoelectric transducer is rigidly attached to an infinite substrate that "sucks" energy out of the

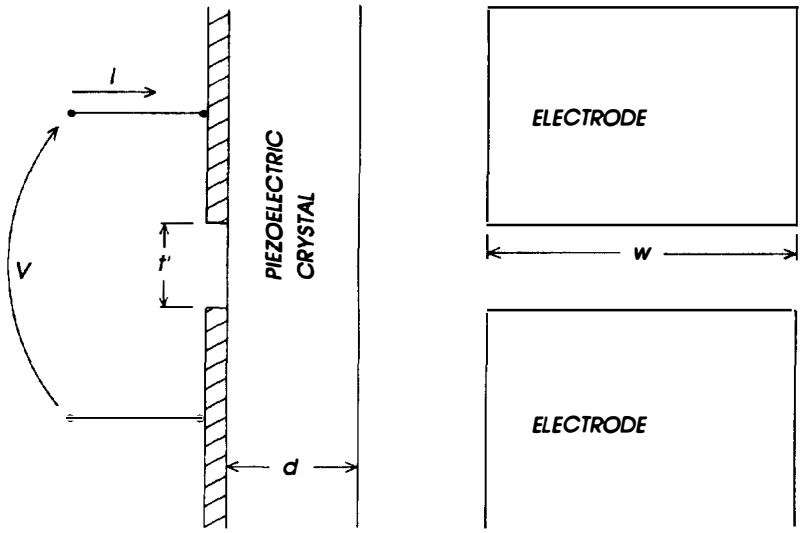

Figure 10.4 Practical realization of LFE resonator. For high frequency application, $d \ll t'$.

transducer. An efficient energy transfer requires a close acoustic impedance match between transducer and substrate (or a quarter-wavelength transformer between them) and a high transducer coupling constant. Further, in wideband applications, a primary goal is matching the acoustic radiation resistance to the electrical source resistance (usually 50 Ω) to achieve maximum power transfer. The reactance of the device is capacitive if the acoustic mismatch between transducer and substrate is not too large, and thus the impedance characteristic is usually in the bottom half of the Smith chart. The resonance condition (5.55) corresponds to the frequency of maximum radiation resistance, which in turn represents the largest energy transfer.

In the resonator configuration, the acoustic wave is confined to the piezoelectric transducer. The radiation resistance is thus zero, at least in this idealized case, which assumes a lossless crystalline material. From inspection of (10.12) and (10.28), it is clear that the impedance (and admittance) is always imaginary as long as the propagation constant k is real. However, because of the tangent function, the reactance can be inductive as well as capacitive; indeed, resonators are most useful in the inductive region. It is thus intuitively clear that the resonance condition in either the TE or LFE resonator structures must have a different interpretation

than in the wideband configuration, because (ideally) there is no energy transfer.

10.4 THE COUPLING CONSTANT AND THE *C* RATIO

In this section, we investigate the physical interpretations of the resonance conditions for TE and LFE configurations. We first consider the TE case. From (10.12), the impedance is infinite when

$$\frac{\theta}{2} = \frac{kd}{2} = \frac{\pi}{2} \tag{10.34}$$

Just as infinite impedance corresponds to a parallel resonance of a lossless electrical circuit, (10.34) corresponds to a series of acoustic frequencies, called *antiresonances*, given by

$$\omega_a = \frac{\pi v_a}{d}(N), \quad N = 1, 3, 5, \ldots \tag{10.35}$$

The anitresonances are harmonically related. Indeed, (10.35) is identical to the resonant frequencies of the wideband configuration (5.55). The correspondence between the resonator antiresonances and the wideband resonances is further strengthened by the fact that the latter also produce maximal device resistance.

We define the "series" resonant frequency similarly by requiring that $Z_{\text{in}} = 0$. From (10.12);

$$1 = k_t^2 \frac{\tan(\theta/2)}{\theta/2} \tag{10.36}$$

Equation (10.36) is a transcendental equation and generally does not have a simple closed-form solution. If the coupling constant k_t is small, then the solutions are close to the poles of the tangent function, and the series resonance frequencies are close to the antiresonances. It is then reasonable to expand the tangent function about its poles. Near the Nth pole, the tangent function can be approximated by

$$\tan\left(\frac{\theta}{2}\right) \approx \frac{4\theta}{(N\pi)^2 - \theta^2} \tag{10.37}$$

For the first pole (fundamental resonance), Equation (10.36) becomes

$$8k_T^2 = \pi^2 - \theta^2 \tag{10.38}$$

Using (10.34), we write

$$\omega_r = \frac{v_a}{d}(\pi^2 - 8k_t^2)^{1/2} \tag{10.39}$$

where ω_r is the resonance frequency. Notice that as $k_t \to 0$, $\omega_a \to \omega_r$. Further, from (10.35) and (10.39), it is clear that $\omega_a \geq \omega_r$.

The difference between the antiresonance and resonance frequencies depends only on the coupling constant. From (10.35) and (10.39),

$$\begin{aligned}\omega_a^2 - \omega_r^2 &= \pi^2\left(\frac{v_a}{d}\right)^2 - \left(\frac{v_a}{d}\right)^2(\pi^2 - 8k_t^2) \\ &= 8k_t^2\left(\frac{v_a}{d}\right)^2\end{aligned} \tag{10.40}$$

If the fractional difference between the frequencies is small, then

$$\omega_a^2 - \omega_r^2 \sim \frac{\omega_a - \omega_r}{2\omega_a}$$

and (10.40) becomes

$$\frac{\omega_a - \omega_r}{\omega_a} = \frac{4k_t^2}{\pi^2} \tag{10.41}$$

Using (10.37) for the Nth pole, we find that the frequency separation between the resonance and antiresonance frequencies is

$$\frac{\omega_a - \omega_r}{\omega_a} = \frac{4k_t^2}{(N\pi)^2}, \quad N = 1, 3, 5 \ldots \tag{10.42}$$

Comparing (10.42) with (10.41), we see clearly that the frequency separation has been effectively reduced by the square of the harmonic number. Alternatively, the effective coupling constant has been reduced by the square of the harmonic number. This analysis is valid only if the coupling constant is small, however. Ferroelectric crystals, such as $LiNbO_3$, which have very high electromechancial coupling, require a graphical or computer analysis of the transcendental equation (10.36).

For lateral-field-excited resonators, the analysis is similar. The *series* resonant frequencies occur when the admittance becomes infinite, and they are given by (10.35). Like the antiresonances of the thickness-excited modes, these frequencies are harmonically related. The *anti*resonances are given by the right side of (10.36) with K^2 replacing k_t^2. Similarly, the frequency separation is given by (10.42), again with k_t replaced by K. For TE and LFE, the antiresonant frequencies are higher than the resonant frequencies for a given harmonic number. This is consistent with the behavior of the impedance characteristic which traverses the Smith chart clockwise (i.e., from series to parallel resonance). These results are summarized in Table 10.2.

Table 10.2 Resonance Conditions

	Thickness Excitation	*Lateral Field Excitation*
Series resonances	$\frac{v_a}{d}((N\pi)^2 - 8k_t^2)$	$\frac{\pi v_a}{d}N$
Parallel resonances	$\frac{\pi v_a}{d}N$	$\frac{v_a}{d}((N\pi)^2 - 8K^2)$
Frequency separation	$\frac{4k_t^2}{(N\pi)^2}$	$\frac{4K^2}{(N\pi)^2}$

The graphical analysis for the two excitations is shown in Figure 10.5. The resonant and antiresonant frequencies are given by the intersections of the tangent function with the straight line of slope k_t^2. For a given component of the piezoelectric matrix, $K > k_t$ (see (5.49)). However, for a given slope (i.e., coupling constant), the frequency separation of the TE modes is greater than that of the LFE modes. Notice also that the frequency separation for both excitation modes decreases as the harmonic number increases.

Normally the resonator is operated at its series resonance. There is a clear advantage to LFE, because for a given frequency the crystal is thicker in this mode than in the TE mode. Indeed, for high coupling crystals such as $LiNbO_3$, ω_r is up to 20% lower in frequency than the half-wave (antiresonance). This reduction in operating frequency is due to the nature of the resonance and is in addition to the metal loading effect, which, as we shall see in Chapter 11, can be quite serious for high frequency operation. In LFE operation, not only are the series resonances higher for a given thickness, but there is no metal loading effect because there is no metal in the acoustic path.

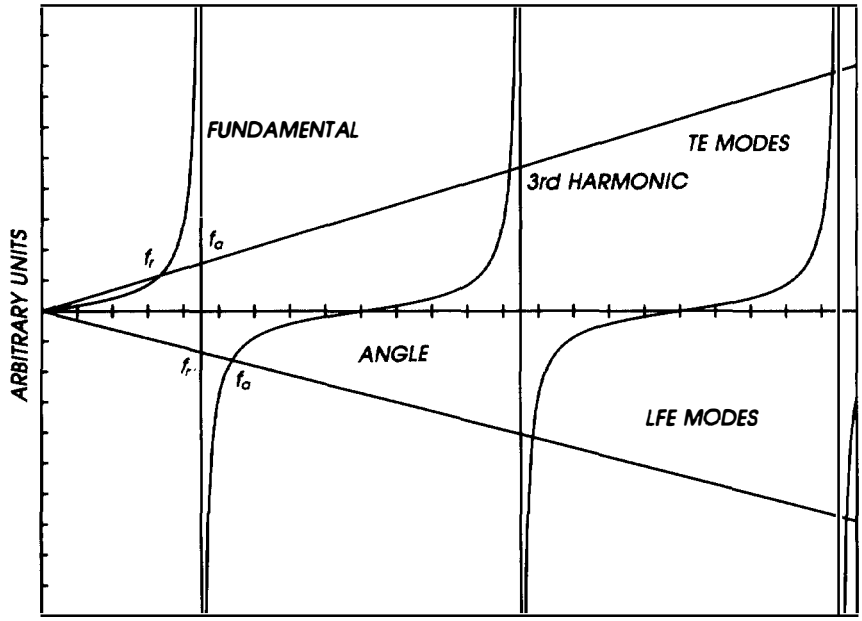

Figure 10.5 Graphical solution of (10.12) and (10.28) showing resonances and antiresonances of piezoelectric resonators for TE and LFE modes.

10.5 BUTTERWORTH-VAN DYKE EQUIVALENT CIRCUIT

From (10.12) or (10.28), it is clear that the resonator can be represented by a constant "clamped" capacitance in parallel with an acoustic or "motional" arm, which can be inductive or capacitive. An equivalent circuit must also reflect the existence of series and parallel resonances, as shown in the previous section. A suitable equivalent circuit, shown in Figure 10.6, is the Butterworth-Van Dyke (BVD) circuit. This circuit is a valid representation for both TE and LFE structures. Figure 10.6(a) shows the equivalent circuit for the fundamental series and parallel resonances. To represent the infinite series of harmonics, we place motional arms in parallel, with each arm corresponding to a discrete N, as shown in Figure 10.6(b). The values of the individual elements determine the series and parallel resonant frequencies for a particular harmonic.

As shown, the circuit does not contain a dissipative element, consistent with (10.12) and (10.28). Later, a resistor, which provides for energy

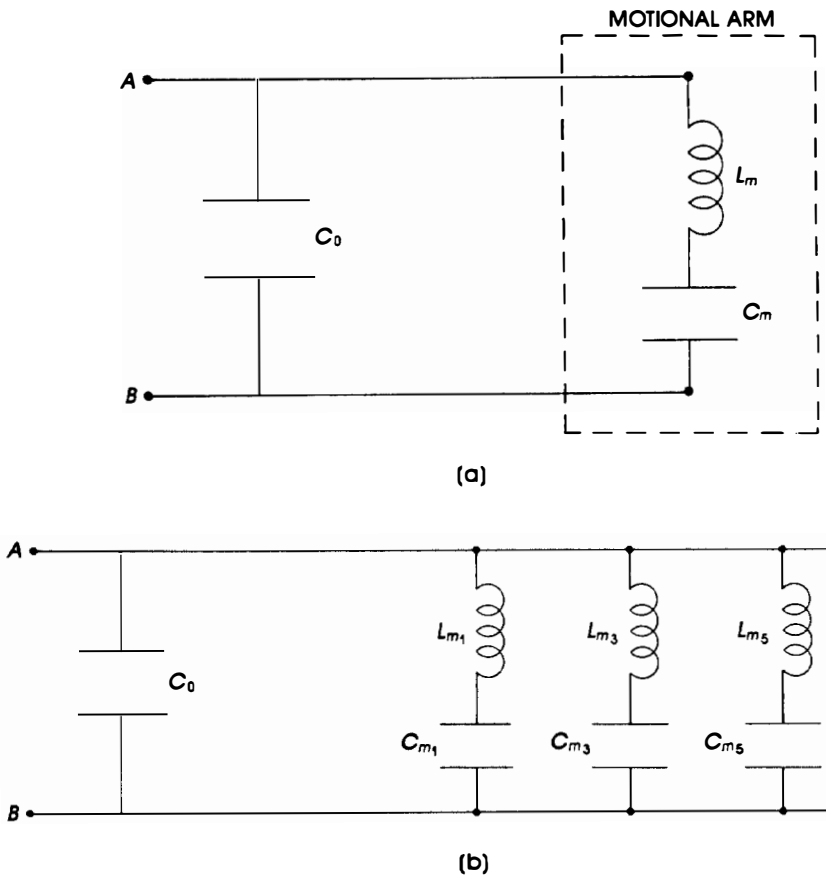

Figure 10.6 Butterworth-Van Dyke equivalent circuit for resonator with no acoustic attenuation: (a) fundamental resonance; (b) harmonic modes with each motional arm representing one mode.

absorption in the device, will be added to the motional arm. For the fundamental mode, the input admittance between terminals A and B is

$$Y_{\text{in}} = Y_{\text{AB}} = j\omega C_0 + \frac{1}{j(\omega L_m - 1/\omega C_m)}$$
$$= \frac{-(\omega L_m - 1/\omega C_m)\omega C_0 + 1}{j(\omega L_m - 1/\omega C_m)} \tag{10.43}$$

The impedance is

$$Z_{\text{in}} = Y_{\text{in}}^{-1} = \frac{j(\omega L_m - 1/\omega C_m)}{1 - \omega^2 C_0 L_m + C_0/C_m} \tag{10.44}$$

Series resonance requires that the impedance be zero:

$$\omega_r = \frac{1}{\sqrt{L_m C_m}} \tag{10.45}$$

Parallel or antiresonance occurs when the impedance is infinite (assuming no resistive element):

$$\omega_a = \sqrt{\frac{C_m + C_0}{L_m C_0 C_m}} = \frac{1}{\omega_r}\sqrt{\frac{C_m + C_0}{C_0}} \tag{10.46}$$

From (10.45) and (10.46), we form the ratio:

$$\frac{\omega_a^2 - \omega_r^2}{\omega_a^2} \approx \frac{\omega_a^2 - \omega_r^2}{\omega_r^2} = \frac{C_m}{C_0} \approx \frac{2(\omega_a - \omega_r)}{\omega_r} \tag{10.47}$$

Comparing (10.47) with (10.41), we infer that for the Nth harmonic,

$$\frac{C_m}{C_0} = \frac{8k_t^2}{N^2\pi^2} \quad \text{(thickness-excited modes)} \tag{10.48}$$

$$\frac{C_m}{C_0} = \frac{8K^2}{N^2\pi^2} \text{ (lateral-field-excited modes)} \tag{10.49}$$

The ratio of the clamped capacitance to the motional capacitance is called the *C ratio* (C_r) and is a FOM of the resonator. A resonator with a small C_r is inductive for a large frequency band. This feature facilitates the design of wideband filters and allows oscillators to be "pulled" by external tuning elements over the inductive frequency band. Typical values of C_r range from less than 4 (for high coupling piezoelectric crystals such as $LiTaO_3$) to well over 1000 (for crystal quartz operating at a high harmonic mode). Note that the C ratio does *not* depend on frequency. Because there is no dissipative element in the equivalent circuit, the input impedance traverses the outer rim of the Smith chart. For each N, the device looks like a short (point 2 in Figure 6.1) at the series resonance and like an open at the parallel resonance (point 1 in Figure 6.1). As N increases, the frequency separation between the two points decreases. In all cases, the device return loss is precisely zero.

10.6 ACOUSTIC ATTENUATION AND THE MOTIONAL RESISTANCE

Until now, our electrical model contained only reactive components. Such a device cannot dissipate energy; thus, it possesses an *infinite Q*. The input impedance is reactive over the entire frequency range (except at the series resonances, where it is zero, and at antiresonance, where it is infinite). A realistic model must incorporate the dissipation not only in the crystal (through acoustic attenuation) but in the metallic layers (through acoustic attenuation and ohmic losses). In this section, we investigate the effect of acoustic attenuation in the crystal material.

We consider the lateral-field-excited modes, although all of the equations are valid for both LFE and TE modes. Recall (10.28):

$$\begin{aligned} Y_{\text{in}} &= j\omega C_0\left(1 + K^2 \frac{\tan(kd/2)}{kd/2}\right) \\ &= j\omega C_0 + j\omega C_0 K^2 \frac{\tan(kd/2)}{kd/2} \\ &= Y_{C_0} + Y_m \end{aligned} \tag{10.50}$$

Clearly, the first term is always reactive, and if the propagation constant k is real, then the motional admittance Y_m is also reactive. If, however, k is complex, then Y_m contains a resistive component. We investigate the motional term under the assumption that

$$\hat{k} = k_{\text{r}} + jk_{\text{i}} \tag{10.51}$$

where k_{r} and k_{i} are the real and imaginary components of the propagation constant. For all practical cases,

$$k_{\text{i}} \ll k_{\text{r}} \tag{10.52}$$

The motional component of the input impedance including a complex k is shown in Figure 10.7. Our task is to derive an expression for the motional resistance in terms of the acoustic and electrical parameters of the piezoelectric crystal. Consider the motional impedance. Using (10.50) and (10.51), we have

$$\frac{1}{Y_m} = Z_m = \frac{1}{j\omega C_0 K^2} \frac{\hat{k}d}{2} \cot\left(\frac{\hat{k}d}{2}\right) \tag{10.53}$$

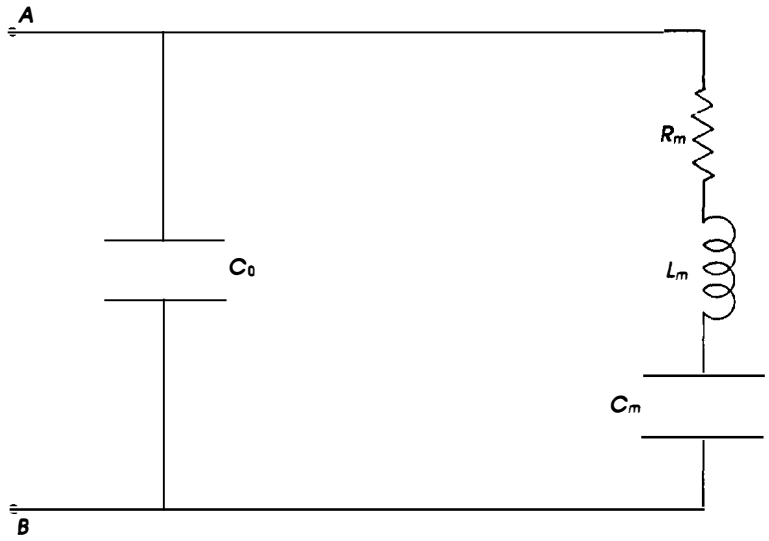

Figure 10.7 Butterworth-Van Dyke equivalent circuit for resonator with attenuation represented by the motional resistance element R_m.

We have previously derived an expression for k_i in terms of the acoustic viscosity η (from (1.22)):

$$k_i = \frac{\eta\omega^2}{2\rho v_a^3} = \frac{\eta\omega}{2\rho v_a^2}\left(\frac{\omega}{v_a}\right)$$

Using (10.52), we assume that the only effect of k_i is to attenuate the acoustic wave; thus,

$$k_r = \frac{\omega}{v_a} \tag{10.54}$$

Using (10.54) and (1.22) in (10.51), we have

$$\hat{k} = \frac{\omega}{v_a}(1 + j\alpha) \tag{10.55}$$

where

$$\alpha = \frac{\eta\omega}{2\rho v_a^2} \text{ and } \alpha \ll 1$$

At series resonance (ω_r), the impedance is purely resistive (but greater than zero):

$$\omega_r: \quad \frac{\hat{k}d}{2} = \frac{\pi}{2}(1 + j\alpha) \tag{10.56}$$

Substituting (10.56) into (10.53), we assume that the imaginary component effects only the cotangent term:

$$\omega_r: \quad Z_m \rightarrow R_m = \frac{(\pi/2)\cot(\hat{k}d/2)}{jK^2\omega_r C_0} \tag{10.57}$$

where

$$\cot\left(\frac{\hat{k}d}{2}\right) = \cot\left(\frac{\pi}{2}(1 + j\alpha)\right) \tag{10.58}$$

Using the trigonometric identity:

$$\cot(A + B) = \frac{\cot(A)\cot(B) - 1}{\cot(A) + \cot(B)} \tag{10.59}$$

in (10.58), we get

$$\cot\left(\frac{\pi}{2}(1 + j\alpha)\right) = \tan\left(j\alpha\frac{\pi}{2}\right) \approx j\alpha\,\frac{\pi}{2} \tag{10.60}$$

because $\alpha \ll 1$. Substituting (10.60) into (10.57), we have

$$R_m = \frac{(\pi/2)^2\alpha}{K^2\omega_r C_0} \tag{10.61}$$

Equation (10.61) is valid for TE modes with the substitution $K \rightarrow k_t$. Using (10.55), we get

$$R_m = \frac{(\pi/2)^2\eta}{2K^2\rho v_a^2 C_0} \tag{10.62}$$

For the thickness modes, C_0 is the capacitance of a parallel plate capacitor, and the motional resistance becomes

$$R_m = \frac{\pi \eta \epsilon_r \epsilon_0}{8 k_T^2 \rho A \omega v_a} \tag{10.63}$$

where A is the electrode area and ω is the operating frequency.

Optimal resonator operation requires designing the motional resistance well below 50 Ω (so that the device does not absorb energy), but not so low that R_m is swamped by external package resistances of bond wires. The only factor in (10.63) under the device designer's control is the area A. As the area decreases, R_m increases. The loss (which depends only on η) has not increased, but the device looks more lossy, at least at series resonance. The parallel resistance also increases, however. This behavior is consistent with our experience with wideband operation in which a decreased area increases R_a (recall that wideband resonance corresponds to resonator antiresonance). Of particular interest (and certainly not intuitively apparent) is the fact that the motional resistance for thickness modes varies inversely with frequency. As the frequency increases, we expect a device to become more lossy (i.e., resistive). At series resonance, just the opposite occurs! The reason is that as ω increases the increase in C_0 (for a constant area) swamps the higher attenuation. The resistance decreases for both the series and parallel resonances (just as the resistance increased for both with decreased area), and so the device is indeed more lossy. This behavior highlights another potential advantage of LFE operation in which C_0 is not necessarily inversely proportional to frequency. In harmonic operation, the coupling constant is reduced by N^2, where N is the harmonic, and thus the motional resistance is increased by a corresponding amount.

Example 10.3. Show the dependence on the transducer area of the input impedance for a typical resonator operating in TE mode. The characteristic of an $\langle AT \rangle$ quartz resonator operating in the third harmonic is shown in Figure 10.8. The operating frequency is 1 GHz and the thickness is 4.8 μm. Curve 1 corresponds to an area of 1×10^{-6} m^2, and curve 2 to an area of 8.8×10^{-8} m^2. Note that the loops are approximately equal in size and conform to the principle that large A implies low R_m for both resonance and antiresonance frequencies.

For a given resonant frequency and electrode area, the material parameters affect the motional resistance according the value of $\eta/k_t^2 \epsilon_r c^E$. The specific value of each of these constants depends on the crystal cut as well as on the crystal material. We can get a feel for the material variation

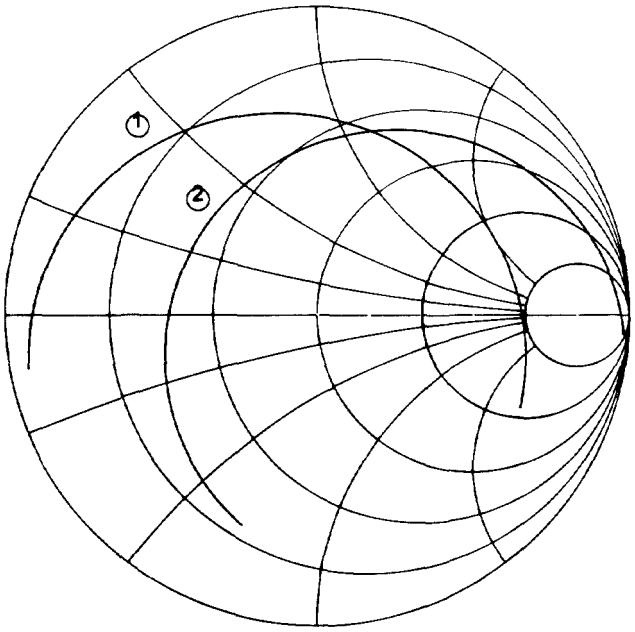

Figure 10.8 Effect of the variation in the resonator area on R_m. The curves show the input impedance for the third harmonic $\langle AT \rangle$-cut with $d = 4.8$ μm. Curve 1 area $= 1 \times 10^{-6}$ m^2, and curve 2 area $= 8.8 \times 10^{-8}$ m^2. Increasing the area decreases R_m for both resonance and antiresonance.

by considering $LiNbO_3$ (high dielectric, high coupling constants, and low viscosity) and α quartz (low dielectric, low coupling constants, and moderate viscosity). The ratios are summarized in Table 10.3.

Table 10.3

	$\frac{LiNbO_3}{\alpha\ quartz}$
k_t^2	25–30
ϵ_r	8–10
c^E	2–3
η	.2–.4

Using the values in Table 10.3 in (10.63), we see that the resistance of a $LiNbO_3$ resonator will be from two to more than three orders of magnitude lower than the resistance for a comparable quartz device. This discrepancy must be accounted for in device designs, especially at high frequencies, where computer simulation (which we investigate in Chapter 11) yields motional resistance values for $LiNbO_3$ of only a few milliohms at 1 GHz.

The values of C_m and L_m can also be computed from fundamental acoustic and electric parameters. Using (10.48), we write the motional capacitance at the fundamental series resonance (for TE modes):

$$C_m = \frac{8}{\pi^2} k_t^2 C_0 = \frac{8\epsilon_r \epsilon_0 A \omega_r}{\pi^3 v_a} k_t^2 \tag{10.64}$$

We can find the motional inductance L_m by solving

$$\omega_r^2 = \frac{1}{L_m C_m} \tag{10.65}$$

for L_m and using (10.64):

$$L_m = \frac{\pi^3 v_a}{8\omega_r^3 \epsilon_r \epsilon_0 A k_t^2} \tag{10.66}$$

10.7 QUALITY FACTOR OF A RESONATOR

We previously derived an expression for the Q of a crystal based on the definition,

$$Q = \frac{(\omega)\ \text{Energy stored}}{\text{Energy dissipated per cycle}}$$

We found that

$$Q = \frac{v_a \rho}{\omega \eta}$$

From the BVD model, the series resonant Q is

$$Q = \frac{\omega_r L_m}{R_m} \tag{10.67}$$

Substituting for L_m and R_m from (10.63) and (10.66) gives

$$Q = \omega_r \underbrace{\left(\frac{\pi^3 v_a}{8\omega_r^3 \epsilon_r \epsilon_0 A k_T^2} \right)}_{L_m} \underbrace{\left(\frac{8k_t^2 \rho A \omega_r v_a}{\pi \eta \epsilon_r \epsilon_0} \right)}_{R_m^{-1}} = \frac{v_a^2 \rho}{\omega_r \eta} \tag{10.68}$$

The material Q of a crystal is identical to the "circuit" Q of the acoustic resonator model, as we expected. This is valid only because we did not consider the effects of the metallic electrodes. In this simplified model, the resonator Q depends only on the crystal properties and is inversely proportional to frequency. Important Q factors are shown in Table 10.4.

Table 10.4

Material	Q (at 1 GHz)	*Mode and Cut*
YAG	240×10^3	⟨1, 0, 0⟩ long.
Spinnel ($MgOAl_2O_3$)	260×10^3	⟨1, 1, 1⟩ shear
$LiTaO_3$	300×10^3	⟨0, 0, 1⟩ long.
$LiNbO_3$	100×10^3	⟨1, 0, 0⟩ long.
Si	3×10^3	⟨1, 0, 0⟩ long.
GaAs	2.3×10^3	⟨1, 0, 0⟩ long.
Crystal quartz	27×10^3	⟨*AT*⟩ shear
Fused quartz	20×10^3	Long.
Al	2×10^3	Long.
Au	480	Long.
Au	250	Shear
Ag	400	Long.

For single crystals, these values represent the highest that can be achieved. The actual Q depends strongly on the crystal cut. Note that the Q of crystal quartz is not among the highest values.

10.8 RESONATOR FIGURE OF MERIT

The figure of merit (FOM) is defined as

$$\text{FOM} = \frac{Q}{2C_r} \tag{10.69}$$

(some authors omit the 2). Because C_r is independent of frequency and Q varies as f^{-1}, the FOM also varies inversely with frequency. There is no protocol for specific device applications, as in acousto-optics where three figures of merit are defined. It is clear, however, that for frequency control applications the FOM is weighted toward high Q (with a probable requirement for temperature stability), whereas for wideband filters the FOM will be weighted toward low capacitance ratio. However, for oscillators, low C_r permits efficient external frequency pulling (as explained below), and for filter applications high-Q resonators decrease the filter insertion loss.

10.9 FREQUENCY PULLING

Consider the circuit in Figure 10.9. The impedance between points A and B is

$$Z_{AB} = \underbrace{\frac{j(\omega L_m - 1/\omega C_m)}{1 - \omega^2 C_0 L_m + C\ C_m}}_{\substack{\uparrow \\ \text{resonator} \\ \text{impedance}}} + \underbrace{\frac{1}{j\omega C_1}}_{\substack{\uparrow \\ \text{external} \\ \text{capacitor}}} \tag{10.70}$$

Simplifying (10.70) gives

$$Z_{AB} = \frac{\omega C_1(1/\omega C_m - \omega L_m) + (1 - \omega^2 C_0 L_m + C_0/C_m)}{(1 - \omega^2 C_0 L_m + C_0/C_m) j\omega C_1} \tag{10.71}$$

At resonance, $Z_{AB} \rightarrow 0$. From (10.71),

$$0 = -\omega_r^2 C_1 L_m + \frac{C_1}{C_m} + 1 - \omega_r^2 C_0 L_m + \frac{C_0}{C_m} \tag{10.72}$$

Solving (10.72) for ω_r, we have

$$\omega_r^2 = \frac{(C_1 + C_0) + C_m}{C_m L_m (C_1 + C_0)} = \frac{1}{L_m C_m} + \frac{1}{L_m (C_0 + C_1)} \tag{10.73}$$

The resonant frequency has been raised by the addition of the series capacitor. Comparing (10.71) with (10.44), we see clearly that the anti-resonant frequency remains unchanged, and thus the two frequencies have been brought closer together; i.e., the capacitance ratio has been increased.

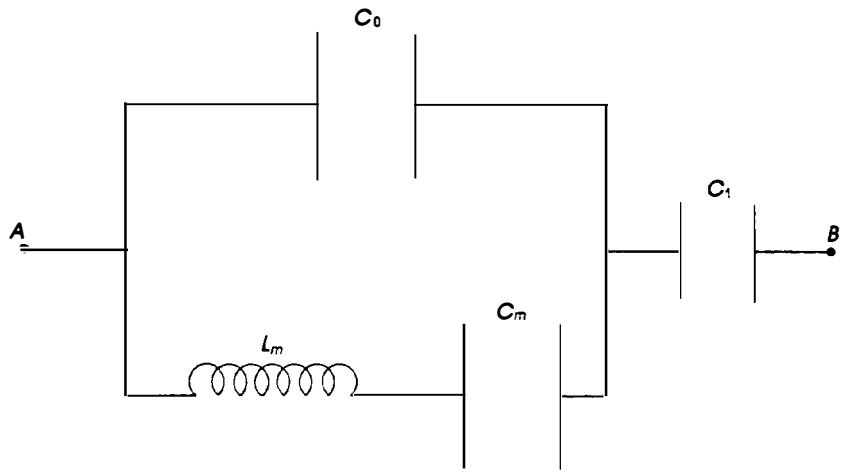

Figure 10.9 Equivalent circuit for resonator with series capacitor. If C_1 is variable, the resonance frequency is increased (in the inductive region) without affecting the antiresonance.

The resonant frequency can only be "pulled" between ω_r and ω_a (which, as we have seen, is the inductive region). Adding a series capacitor enables the device to be tuned to a desired frequency at the expense of increased C_r. Adding a series inductor will lower ω_r (and therefore reduce C_r) at the expense of lowering the overall Q (because external inductors usually have rather low Q-factors). The addition of a parallel capacitor has the effect of decreasing the antiresonance frequency without changing the resonance frequency. Indeed, one reason why antiresonances are not used in oscillator circuits (besides the fact that it is difficult to design an oscillator around a high resistance element) is that the frequency of such a circuit would be subject to variations in the stray capacitances.

10.10 CRYSTAL QUARTZ

Crystal quartz is the most important resonator material presently available. It has been used for over 50 years, and thus growth, characterization, and fabrication techniques are quite mature. Its low coupling is usually not a disadvantage when it is used for frequency control applications. For reasonable values of transducer area, the resistance falls in the 10–20-Ω range at 5–20 MHz. This range is ideal for oscillator circuits. Its Q is somewhat lower than for ferroelectric materials, but at low frequencies

it is more than adequate, and because the stoichiometry of crystal quartz is simple and its growth technology well established, there are few crystal defects and the attenuation has a frequency squared dependence. Only when very high frequencies or wide inductive regions are required do designers look beyond quartz.

The slowness curves for the *xy* and *yz* planes are shown in Figures 10.10 and 10.11. In the *xy* plane the curves are symmetric (which is also true in the *xz* plane), but in the *yz* plane they are not. Power flow angle curves in the *xy* and *yz* planes are shown in Figure 10.12. In the *xy* plane, not only are there no pure modes, but all modes have finite power flow angles. As is characteristic of the trigonal symmetry, in the *xz* plane there is a pure shear mode with a slowness curve that is a rotated ellipse and thus has a finite power flow angle. Figures 10.13 and 10.14 show the coupling constant (in this case k_t^2) in the *xy* and *yz* planes. In the *xy* plane, all modes are excited, but in the *yz* plane there is only one excited mode, the pure shear mode. This behavior contrasts with that in $LiNbO_3$, where only the quasishear mode is excited in the *yz* plane. Although both crystals are trigonal, they belong to different classes and their piezoelectric matrices have different forms (Chapter 4). The curves are labeled *a*, *b*, and *c* rather than quasilongitudinal and quasishear to conform to resonator notation. The explanation of the letters is simply that *a* belongs to the highest velocity, *b* to the middle velocity, and *c* to the smallest velocity. Usually, *a* corresponds to the quasilongitudinal mode, *b* to the fast shear mode (the pure mode, e.g., in cubic symmetry), and *c* to the slow (quasi) shear modes.

When a shear degeneracy occurs, the coupling constant curves jump, as shown in Figure 10.14. In reality, the curves are continuous. Consider, for example, the coupling constant curve in the *yz* plane. From Figure 10.11, there are two points of shear degeneracy: one along the *z*-axis, and one at 156° from the *y*- to *z*-axes. Only the pure shear mode is excited, but between 90° and 156° it is called the *c* mode, and elsewhere it is known as the *b* mode. We will encounter similar discontinuities in Chapter 11, which are understood in the same way. Because there is only one excited mode, which is a pure mode, the *yz* plane is quite important. There are four widely used cuts in this plane: The *AC*- and *BC*-cuts represent orientations with zero power flow angle; the ⟨*AT*⟩- and ⟨*BT*⟩-cuts have finite power flow angle but excellent thermal properties. According to the convention used in crystal resonators, the angles with respect to the *y*-axis are measured in the opposite sense to the convention employed here [1].

The popular ⟨*AT*⟩- and ⟨*BT*⟩-cuts are examples of singly rotated orientations, because their plate normals do not have a component in the *x* direction. These cuts are obtained by rotating the bulk crystal around the

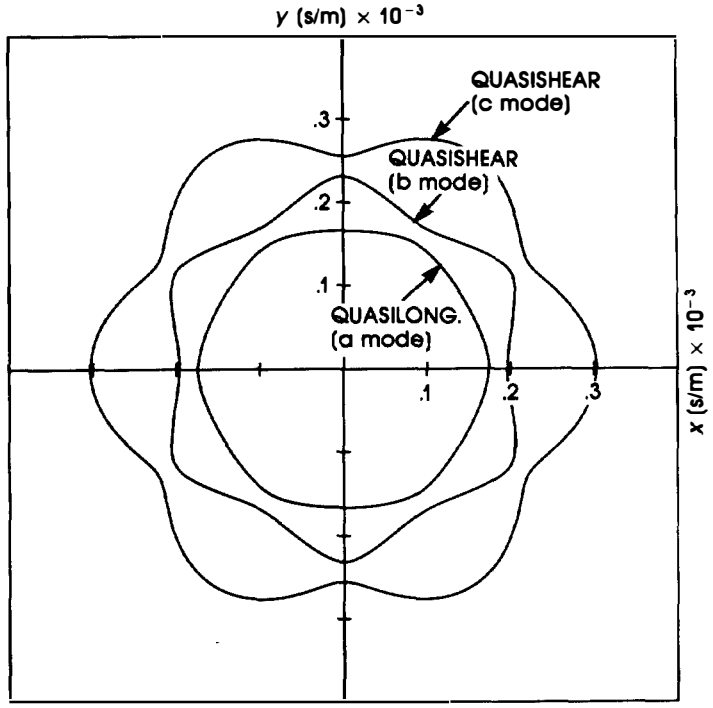

Figure 10.10 Slowness curves of crystal quartz in the xy plane.

x-axis at angles of 145° and 49°, respectively. There are also interesting *doubly* rotated cuts, the most important of which is the $\langle SC \rangle$- (or stress compensated) cut. Unlike the $\langle AT \rangle$ or $\langle BT \rangle$, in the $\langle SC \rangle$-cut all modes are excited, although the c mode is most useful because of its desirable thermal properties. All the modes are quasimodes with finite power flow angles and relatively low coupling constants. There are, however, advantages to the $\langle SC \rangle$-cut, chief among them being its insensitivity to accelerations, which is extremely important in military applications.

10.11 THERMAL STABILITY

The performance of crystal oscillators ultimately is determined by the ability of the resonator to remain on the desired frequency, even under difficult environmental situations. The two most important factors are

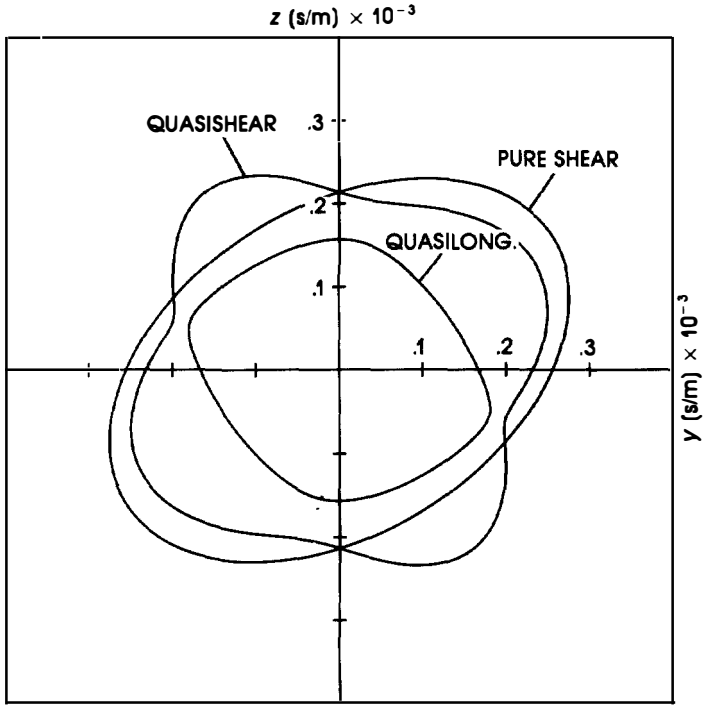

Figure 10.11 Slowness curves of crystal quartz in the *yz* plane. Note the lack of symmetry in this plane, compared with Figure 10.10.

temperature variations and accelerations. In this section, we examine the temperature dependence. As we have seen, the resonant frequency depends on the crystal thickness, phase velocity, and, possibly, the electromechanical coupling constant. This dependence is written as

$$f_r = \sqrt{\frac{c}{\rho}} \frac{1}{2d} \tag{10.74}$$

where c is the (piezoelectrically stiffened) stiffness constant of the excited mode, ρ is the material density, and d is the crystal thickness. Equation (10.74) is valid only for the (fundamental) series resonance of LFE modes or the parallel resonance of *TE* modes. Because the factors in (10.74) are all temperature-dependent, frequency stability requires a cancellation of

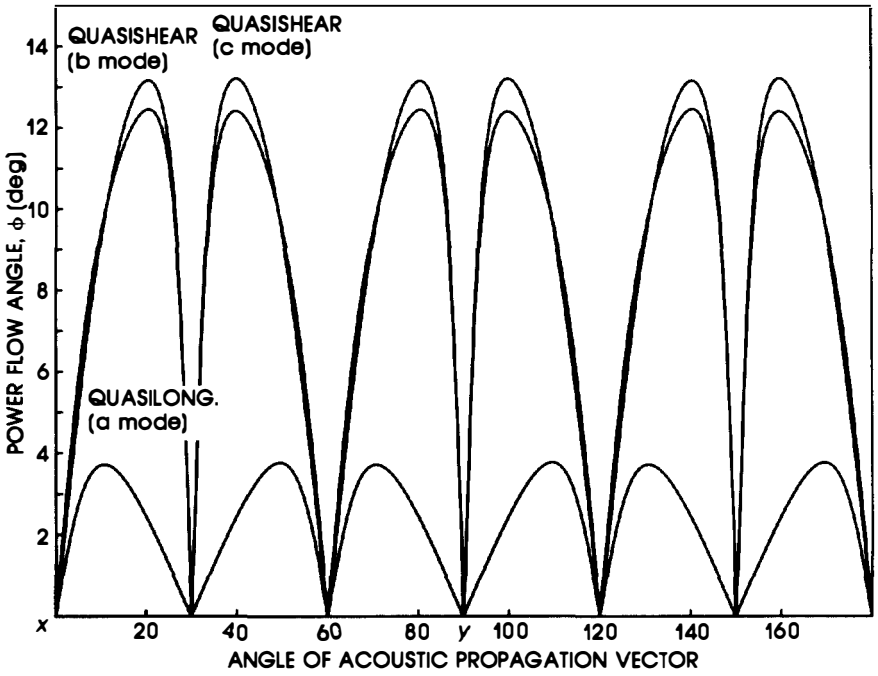
QUASISHEAR
(b mode)
QUASISHEAR
(c mode)
QUASILONG.
(a mode)
POWER FLOW ANGLE, ϕ (deg)
14
12
10
8
6
4
2
x
20
40
60
80
y
100
120
140
160
ANGLE OF ACOUSTIC PROPAGATION VECTOR

(a)

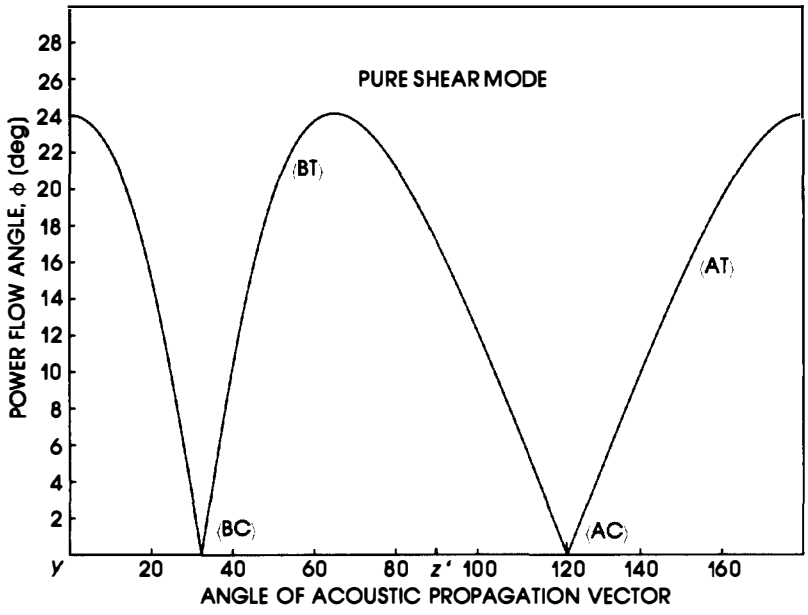
PURE SHEAR MODE
⟨BT⟩
⟨AT⟩
⟨BC⟩
⟨AC⟩
POWER FLOW ANGLE, ϕ (deg)
28
26
24
22
20
18
16
14
12
10
8
6
4
2
y
20
40
60
80
z'
100
120
140
160
ANGLE OF ACOUSTIC PROPAGATION VECTOR

(b)

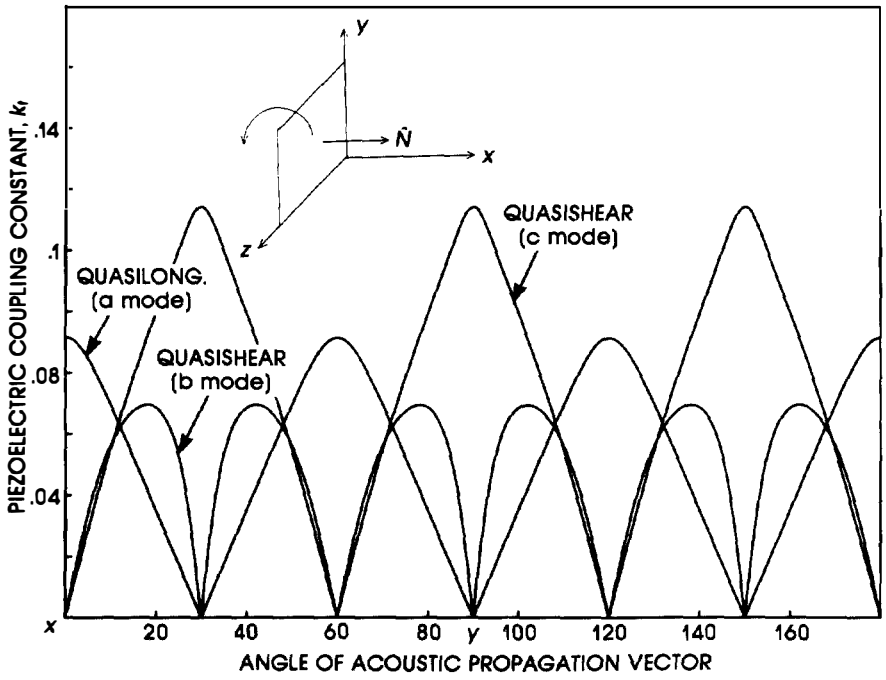

Figure 10.13 Coupling constant of crystal quartz in the xy plane (TE excitation). All modes are excited.

the dependency. Temperature stability refers to the determination of those crystal orientations (crystal "cuts") in which various dependencies cancel each other.

Differentiating (10.74), we obtain

$$\frac{1}{f_r}\frac{\mathrm{d}f_r}{\mathrm{d}T} = \frac{1}{2}\left[\frac{1}{c}\frac{\mathrm{d}c}{\mathrm{d}T} - \frac{1}{\rho}\frac{\mathrm{d}\rho}{\mathrm{d}T}\right] - \frac{1}{d}\frac{\mathrm{d}d}{\mathrm{d}T} \tag{10.75}$$

The last term represents the temperature variation of the resonator thickness. This term is determined by the linear coefficient of expansion α, which varies with direction in the same fashion as the permittivity. Thus, in all classes up to orthorhombic, the coefficient of expansion can be represented by a diagonal 3×3 matrix with either one (for isotropic and cubic classes), two (for tetragonal, hexagonal, and trigonal classes), or three (for the orthorhombic symmetry) components.

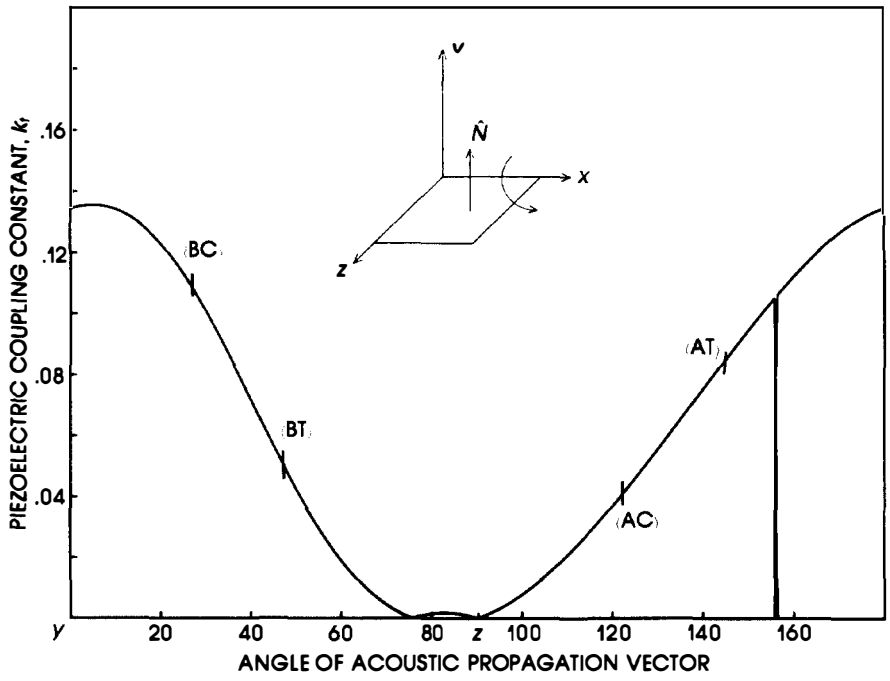

Figure 10.14 Coupling constant of crystal quartz in the *yz* plane (TE excitation). Only the pure shear mode is excited. The "jumps" occur because the mode changes from fast (*b* mode) to slow (*c* mode) shear mode at 156° (see Figure 10.11).

For crystal orientation along one of the principal axes, we easily determine the corresponding α component by inspection. For off-axis orientation, α is given by (compare (4.46)):

$$\alpha = \frac{1}{d}\frac{\mathrm{d}d}{\mathrm{d}T} = l_i \alpha_{ij} l_j \tag{10.76}$$

This term is usually (but not always) positive (an increase in temperature results in an increased thickness) and thus causes the frequency to decrease. Typical values of α range upward to 10^{-6}/°C. Table 10.5 lists some expansion coefficients of important resonator materials.

The middle term in (10.75) represents the temperature variation of the material density. An increase in temperature causes a decrease in

Table 10.5 Linear Expansion Coefficients (times 10^{-6})

Material	α_{11}	α_{22}	α_{33}
Quartz	14.3	14.3	7.48
$AlPO_4$	15.9	15.9	9.7
$LiNbO_3$	15.4	15.4	7.5
$LiTaO_3$	16.2	16.2	4.1

density, because the resonator dimensions increase and the mass clearly does not. As density decreases, the frequency increases, so the effects of resonator thickness expansion and density decrease tend to cancel. From the definition, it is apparent that

$$\frac{1}{\rho}\frac{d\rho}{dT} = \alpha_{11} + \alpha_{22} + \alpha_{33} \tag{10.77}$$

The effect on frequency variation due to density changes is constant with crystal orientation and is usually about 1.5 to 3 times larger than the effect on thickness variations (depending on the crystal cut).

The first term in (10.74) represents the fractional change in resonance frequency due to changes in the stiffness constants with temperature. The fractional change in a c component is called Tc and has units of parts per °C. This term is almost always significantly larger than the others and is, unfortunately, the most difficult to determine. Because each stiffness component can change independently of the others, the phenomenon must be described by a 6×6 matrix that has the same symmetry as the stiffness matrix. Usually, a rise in temperature will make the stiffness components softer and more compliant so that most Tc values are negative. We are interested in the exceptions to this rule, which allow the existence of temperature-stable orientations. Table 10.5 lists three crystals for which values of Tc have been measured.

Table 10.6 Temperature Coefficients of Stiffness Constants (times 10^{-4}/°C)

Material	Tc_{11}	Tc_{33}	Tc_{44}	Tc_{12}	Tc_{13}	Tc_{14}	Tc_{66}
Quartz	−.485	−1.6	−1.77	−30	−5.5	−1	+1.78
$AlPO_4$	−.76	−2.18	−1.57	−15	−4	+.72	+1.03
$LiNbO_3$	−1.74	−1.53	−2.04	−2.52	−1.59	−2.14	−1.43
$LiTaO_3$	−1.03	−.96	−.43	−3.41	−.5	+6.67	−.47

From Table 10.6, it is apparent that in quartz, $AlPO_4$, and $LiTaO_3$ orientations exist for *shear* modes that should be temperature stable. That Tc_{66} is positive for quartz suggests the possibility of a temperature-stable mode for the pure x-polarized shear wave in the yz plane (recall that 6 represents xy). These modes are particularly desirable because their stiffness components can be written in simple form and because they are pure. The stiffness component for an arbitrary direction is

$$c = c_{66}l_y^2 + c_{44}l_z^2 + 2c_{14}l_yl_z \tag{10.78}$$

Multiplying each of the stiffness components by its corresponding temperature coefficient yields the net Tc. The total fractional frequency variation with orientation in the yz plane of quartz for the pure shear mode is shown in Figure 10.15.

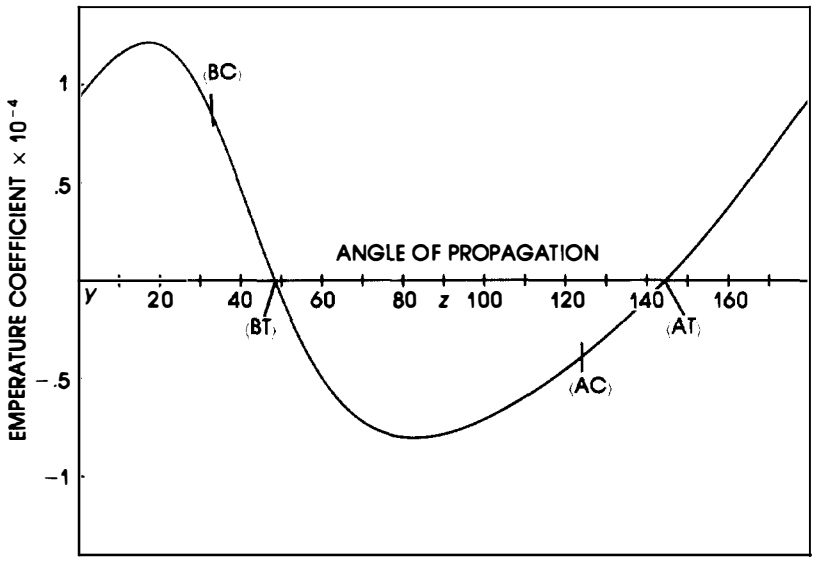

Figure 10.15 Temperature coefficient of frequency for the pure shear mode in crystal quartz in the yz plane. The two stable orientations are called the (AT)- and (BT)-cuts (T stands for temperature).

Two temperature-stable cuts are the AT-cut ($y - 35°$) and the BT-cut ($y + 49°$). It is not an exaggeration to say that the entire resonator

industry owes its existence to Tc_{66}. Figure 10.16 shows the fractional frequency variation with orientation for $LiNbO_3$. As expected, $LiNbO_3$ does not possess any temperature-stable cuts, because all of the individual coefficients are negative. If the stiffness constant cannot be written in closed form as in (10.78), we may use the following strategy:

1. Multiply the individual stiffness components by their corresponding *Tc* values to form a 6 × 6 matrix called **Tc**.
2. Solve the "eigen" *Tc* by solving the Christoffel equation, using the matrix **Tc**. This is done in precisely the same way that we solved the Christoffel equation Chapter 3.
3. Resolve the Christoffel equation for the same orientation ($\hat{\mathbf{l}}$). The desired *Tc* component is simply the ratio of these two terms.

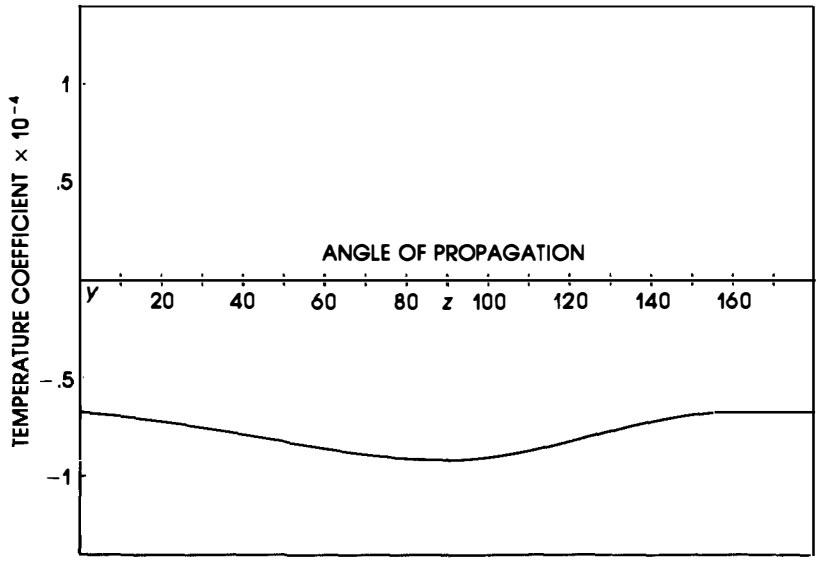

Figure 10.16 Temperature coefficient of frequency for the pure shear mode of $LiNbO_3$ in the *yz* plane. There are no temperature-stable cuts.

PROBLEMS

10.1 Determine the relation between possible stresses and electric fields (see (10.13)) for ⟨*z*⟩ quartz and find the possible TE and LFE modes of excitation.

10.2 Show that there is no longitudinal electric field in LFE of ⟨*z*⟩ ZnO.

10.3 Determine the frequency pulling relations for a series inductor from the BVD equivalent circuit.

10.4 From (10.47), calculate the antiresonance frequency for the resonator of Example 10.2 if the C ratio is 150.

10.5 Derive an equation for the antiresonance frequency of a resonator with a parallel capacitor (for example, package capacitance) placed across it.

10.6 How does placing an inductor in parallel with the resonator affect the resonance and antiresonance frequencies and the C ratio?

10.7 Develop an equation for the motional resistance in terms of resonator Q, using (10.62) and (10.68). What is the approximate Q of an ⟨AT⟩-cut quartz resonator if $A = 1 \times 10^{-6}$ and the external resistance (bond wires, electrode metalization, etc.) is 1 Ω?

REFERENCES

1. V. Bottom, *Introduction to Quartz Crystal Unit Design,* D. Van Nostrand, New York, 1982.
2. R. Heising (ed), *Quartz Crystals for Electrical Circuits,* D. Van Nostrand, New York, 1946.
3. R. Holland and E. Eernisse, *Design of Resonant Piezoelectric Devices,* The MIT Press, Cambridge, 1969.
4. W. Cady, *Piezoelectricity,* Dover, New York, 1964.
5. M. Frereking, *Crystal Oscillator Design and Temperature Compensation,* D. Van Nostrand, New York, 1970.
6. W. Mason, *Piezoelectric Crystals and Their Applications to Ultrasonics,* D. Van Nostrand, New York, 1950.
7. E. Gerber and A. Ballato (eds.), *Precision Frequency Control,* Academic Press, New York, 1985.
8. E. Eernisse, "Quartz Resonator Frequency Shifts Arising from Electrode Stress," *Proc. 29th Annual Frequency Control Symp.,* 1 (1975).
9. A. Ballato, "Piezoelectric Resonators," Chapter 3 in *Design of Crystal and Other Oscillators,* John Wiley and Sons, New York, 1983.